Int. J. Solids Structures, 1976, Vol. 12, pp. 683–691. Pergamon Press. Printed in Great Britain

BUCKLING OF ELASTIC-PLASTIC OVAL CYLINDRICAL SHELLS UNDER AXIAL COMPRESSION

VIGGO TVERGAARD
Department of Solid Mechanics, The Technical University of Denmark, Lyngby, Denmark

(*Received* 9 *February* 1976; *revised* 29 *March* 1976)

Abstract—For an axially compressed elastic-plastic cylindrical shell with elliptical cross-section the buckling behaviour is investigated. The initial post-bifurcation behaviour of a perfect shell compressed into the plastic range is determined in terms of an asymptotic expansion. The behaviour of shells with initial stress free imperfections is computed numerically using an incremental procedure. For shells with sufficiently eccentric cross-sections elastic analyses predict final collapse loads considerably above the bifurcation load, but the present numerical results show that elastic-plastic material behaviour reduces these collapse loads to such an extent that the elastic-plastic shells are moderately imperfection-sensitive.

1. INTRODUCTION

The oval cylindrical shell under axial compression represents an interesting example of more complex post-buckling behaviour in the elastic range. Hutchinson[1] has shown that the initial post-buckling behaviour predicts a severe imperfection-sensitivity. On the other hand, numerical computations of the advanced post-buckling behaviour by Kempner and Chen[2,3] and later by Almroth, Brogan and Marlowe[4] have shown that in the post-buckled range load carrying capacities above the bifurcation load are attained, provided the cross-sections are sufficiently eccentric. Thus, the post-buckling equilibrium load initially decreases strongly, but then starts to grow again until final collapse occurs above the primary buckling load. This behaviour has also been confirmed by experiments[5,6]. In the above mentioned investigations the cross-sectional shapes are either elliptical[1, 4, 5] or a different oval shape[1–3, 6] that is also considered by Kempner and Chen in a recent investigation of an oval cylindrical shell under combined bending and axial compression[7].

The present paper gives an investigation of the post-buckling behaviour of an oval axially compressed cylinder made of an elastic-plastic material. The critical bifurcation load and the corresponding mode are determined by a numerical procedure, and based on this solution Hutchinson's asymptotic theory[8, 9] is employed to obtain asymptotic expressions for the initial post-bifurcation behaviour in the plastic range and for the initial propagation of elastic unloading regions after bifurcation. The behaviour in the advanced post-buckling range and the behaviour of initially imperfect shells is computed numerically by a linear incremental method. The computations show that elastic-plastic material behaviour eliminates the high post-buckling load carrying capacity known from the elastic range.

2. PROBLEM FORMULATION

The cross-sectional shape of the oval cylindrical shell considered here is taken to be elliptical with a major axis of length a and a minor axis of length b (Fig. 1). Then, points on the middle surface can be described by the relations

$$(y, z) = (-a \cos \psi, b \sin \psi), \qquad 0 \le \psi \le 2\pi \tag{2.1}$$

in terms of a parameter ψ. At a point $\psi = \psi_s$ the circumferential distance s from the point $\psi = 0$ and the radius of curvature R_s, respectively, are given by the expressions

$$s = a \int_0^{\psi_s} \sqrt{\left[1 + \left(\frac{b^2}{a^2} - 1\right) \cos^2 \psi\right]} \, \mathrm{d}\psi \tag{2.2}$$

$$R_s = \frac{a^2}{b} \left\{1 + \left(\frac{b^2}{a^2} - 1\right) \cos^2 \psi\right\}^{3/2}. \tag{2.3}$$

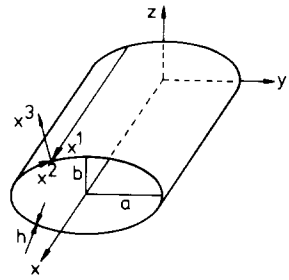

Fig. 1. Cylindrical shell with elliptical cross-section.

In the following we let a point on the shell middle surface be identified by the coordinates $(x^1, x^2) = (x, s)$ and denote the displacements of the shell middle surface by v^α in the directions of the surface base vectors and w in the direction of the outward surface normal. The shell equations used are those given by Niordson[10] with the nonlinear membrane strain tensor

$$\epsilon_{\alpha\beta} = \frac{1}{2}(v_{\alpha,\beta} + v_{\beta,\alpha}) - d_{\alpha\beta}w + \frac{1}{2}a^{\gamma\delta}(v_{\gamma,\alpha} - d_{\gamma\alpha}w)(v_{\delta,\beta} - d_{\delta\beta}w) + \frac{1}{2}(w_{,\alpha} + d_\alpha{}^\gamma v_\gamma)(w_{,\beta} + d_\beta{}^\gamma v_\delta) \tag{2.4}$$

and the linear bending strain tensor

$$\kappa_{\alpha\beta} = w_{,\alpha\beta} + d_{\alpha\gamma}v^\gamma_{,\beta} + d_{\beta\gamma}v^\gamma_{,\alpha} + v^\gamma d_{\gamma\alpha,\beta} - d_{\beta\gamma}d_\alpha{}^\gamma w. \tag{2.5}$$

Here $a_{\alpha\beta}$ and $d_{\alpha\beta}$ are the metric tensor and the curvature tensor, respectively, of the undeformed middle surface, and $(\ )_{,\alpha}$ denotes covariant differentiation. These strain measures are identical with those given by Koiter[11] except for small differences in the bending strain measure of the order of $d_\alpha{}^\gamma \epsilon_{\gamma\beta}$.

A small strain theory of plasticity is used, in which the three dimensional stress rates and strain rates in the shell material are assumed to be related by the equations

$$\dot{\sigma}^{ij} = L^{ijkl}\dot{\eta}_{kl} \tag{2.6}$$

with $L^{ijkl} = L^{jikl} = L^{klij}$, where a dot denotes differentiation with respect to some monotonically increasing parameter that characterizes the loading history. Here, Latin indices range from 1 to 3, while Greek indices range from 1 to 2. The instantaneous moduli L^{ijkl} depend on the stress history, and here it is assumed that they have two branches, one corresponding to plastic loading, the other to elastic unloading. The stress state in the shell is approximately plane. Thus, only the in-plane stresses enter into the stress-strain relations, and we can write

$$\dot{\sigma}^{\alpha\beta} = \hat{L}^{\alpha\beta\gamma\delta}\dot{\eta}_{\gamma\delta} \tag{2.7}$$

where the in-plane moduli are given by

$$\hat{L}^{\alpha\beta\gamma\delta} = L^{\alpha\beta\gamma\delta} - \frac{L^{\alpha\beta 33}L^{\gamma\delta 33}}{L^{3333}} \tag{2.8}$$

and the strain rate at distance x^3 outward from the shell middle surface is approximated by

$$\dot{\eta}_{\alpha\beta} = \dot{\epsilon}_{\alpha\beta} - x^3\dot{\kappa}_{\alpha\beta}. \tag{2.9}$$

Using the usual definitions of the membrane stress tensor $N^{\alpha\beta}$ and the moment tensor $M^{\alpha\beta}$, we find the incremental relations

$$\dot{N}^{\alpha\beta} = H^{\alpha\beta\gamma\delta}_{(1)}\dot{\epsilon}_{\gamma\delta} + H^{\alpha\beta\gamma\delta}_{(2)}\dot{\kappa}_{\gamma\delta}, \qquad \dot{M}^{\alpha\beta} = H^{\alpha\beta\gamma\delta}_{(2)}\dot{\epsilon}_{\gamma\delta} + H^{\alpha\beta\gamma\delta}_{(3)}\dot{\kappa}_{\gamma\delta} \tag{2.10}$$

where

$$H_{(i)}^{\alpha\beta\gamma\delta} = \int_{-h/2}^{h/2} \hat{L}^{\alpha\beta\gamma\delta}(-x^3)^{i-1}\,dx^3. \tag{2.11}$$

The theory of plasticity employed here is small-strain J_2 flow theory with isotropic hardening. In the three dimensional x^i-coordinate system with metric tensor g_{ij} the instantaneous moduli of J_2 flow theory are

$$L^{ijkl} = \frac{E}{1+\nu}\left\{\frac{1}{2}(g^{ik}g^{jl}+g^{il}g^{jk}) + \frac{\nu}{1-2\nu}g^{ij}g^{kl} - f\frac{s^{ij}s^{kl}}{\sigma_e^2}\right) \tag{2.12}$$

where E and ν are Young's modulus and Poisson's ratio, respectively, and

$$s^{ij} = \sigma^{ij} - \frac{1}{3}g^{ij}g_{kl}\sigma^{kl}, \qquad \sigma_e = \left\{\frac{3}{2}g_{ik}g_{jl}s^{ij}s^{kl}\right\}^{1/2} \tag{2.13}$$

$$f(\sigma_e) = \begin{cases} \dfrac{3}{2}\dfrac{E/E_t - 1}{E/E_t - (1-2\nu)/3}, & \text{for } \sigma_e = (\sigma_e)_{\max} \text{ and } \dot{\sigma}_e > 0 \\ 0, & \text{for } \sigma_e < (\sigma_e)_{\max} \text{ or } \dot{\sigma}_e < 0. \end{cases} \tag{2.14}$$

Here the tangent modulus E_t is the slope of a uniaxial stress-strain curve, and the initial value of $(\sigma_e)_{\max}$ is the yield stress σ_y. The uniaxial stress-strain behaviour chosen is a piecewise power law with continuous tangent modulus

$$\epsilon = \begin{cases} \dfrac{\sigma}{E}, & \text{for } \sigma \le \sigma_y \\ \dfrac{\sigma_y}{E}\left[\dfrac{1}{n}\left(\dfrac{\sigma}{\sigma_y}\right)^n - \dfrac{1}{n} + 1\right], & \text{for } \sigma > \sigma_y \end{cases} \tag{2.15}$$

where n is the strain hardening exponent.

3. PLASTIC BIFURCATION AND POST-BIFURCATION BEHAVIOUR

The general treatment of uniqueness and bifurcation in elastic-plastic solids, given by Hill [12, 13], has recently been extended by Hutchinson [8, 9] to a general asymptotic theory of the initial post-bifurcation behaviour in the plastic range. In this asymptotic theory the load in the vicinity of the bifurcation point is expanded in terms of the buckling mode amplitude, similar to what is done in Koiters elastic post-buckling theory [14], but the analysis in the plastic range is further complicated by the necessity to account for elastic unloading.

In the present paper the specialization of Hutchinson's theory to Donnell-Mushtari-Vlasov shell theory [9] is used to determine the initial post-bifurcation behaviour. Thus, the bifurcation and asymptotic results are based on retaining only one of the nonlinear terms, $1/2w_{,\alpha}w_{,\beta}$, in the expression (2.4) for $\epsilon_{\alpha\beta}$ and only the first term, $w_{,\alpha\beta}$, in the expression (2.5) for $\kappa_{\alpha\beta}$. The prebuckling stress state in a perfect oval shell consists of a constant uniaxial stress $\sigma^{11} = \lambda\sigma_0^{11}$ at every point of the shell, and the small values of $w_{,2}^0$ prior to bifurcation are neglected. Later comparison with the numerical results shows that the simplified bifurcation analysis agrees reasonably with that based on more accurate shell theory.

The bifurcation mode for the long axially compressed oval shell is periodic in the axial direction of the form

$$\left.\begin{aligned} \overset{(1)}{v}_1 &= U(s)\sin(Qx) \\ \overset{(1)}{v}_2 &= V(s)\cos(Qx) \\ \overset{(1)}{w} &= W(s)\cos(Qx) \end{aligned}\right\}. \tag{3.1}$$

The mode shape in the circumferential direction is determined numerically by making a finite element approximation of the functions $U(s)$, $V(s)$ and $W(s)$ in terms of Hermitian cubics. The critical bifurcation mode and the critical load parameter λ_c correspond to the smallest value of λ for which a non-trivial solution exists of the homogeneous equations

$$\delta I = 0 \tag{3.2a}$$

$$I = \frac{1}{2}\int_0^{s_M}\int_0^{x_M}\left\{\overset{(1)}{N}{}^{\alpha\beta}\overset{(1)}{\epsilon}_{\alpha\beta} + \overset{(1)}{M}{}^{\alpha\beta}\overset{(1)}{\kappa}_{\alpha\beta} + \lambda N_0{}^{11}\overset{(1)}{w}_{,1}\overset{(1)}{w}_{,1}\right\} dx\, ds = 0 \tag{3.2b}$$

where $N_0{}^{11} = h\sigma_0{}^{11}$, and $\overset{(1)}{N}{}^{\alpha\beta}$ and $\overset{(1)}{M}{}^{\alpha\beta}$ are related to $\overset{(1)}{\epsilon}_{\gamma\delta}$ and $\overset{(1)}{\kappa}_{\gamma\delta}$ by eqn (2.10), with the plastic branch of the tensor of moduli used everywhere. The limits s_M and x_M of the integration area are chosen according to the smallest repeatable intervals in the deformation pattern.

Specially for the circular cylindrical shell compressed into the plastic range the critical bifurcation mode is axisymmetric. Using the expressions E_1, E_2, and E_{12} for the physical values of the plastic branches of $\hat{L}^{1111}$, $\hat{L}^{2222}$ and $\hat{L}^{1122}$, respectively, at the bifurcation point, and using $D_1 = E_1 h^3/12$, we easily find the critical stress σ_C and axial wave number Q_C for the axisymmetric mode in a circular cylinder given by

$$\sigma_C = -\frac{2D_1 Q_C^2}{h}, \qquad Q_C = \sqrt[4]{[\{h/R^2\}\{E_2 - (E_{12})^2/E_1\}/D_1]}. \tag{3.3}$$

For the elliptical cylinder the critical stress σ_E and the corresponding instantaneous moduli are determined iteratively from eqn (3.2), and the axial wave number Q_E is determined numerically as the value of Q that minimizes λ_c. The bifurcation mode is a short-wave pattern in the axial direction with buckling deflections confined mainly to the regions of minimum curvature. Buckling loads corresponding to modes that are symmetric with respect to the minor axis and asymmetric with respect to the major axis are nearly identical with the buckling loads corresponding to modes symmetric with respect to both axes, whereas somewhat higher buckling loads are obtained for modes asymmetric with respect to the minor axis. In the following we shall only consider modes symmetric with respect to both axes. The variation of the critical stress and the axial wave length with aspect ratio b/a is shown in Fig. 2 for elliptical cylinders with $R_b/h = 200$, where $R_b = a^2/b$ is the radius of curvature (2.3) at the ends of the minor axis. Even for rather small aspect ratios there is a reasonable agreement with the simple engineering approximation that bifurcation occurs when the stress reaches the critical stress for a circular cylinder with radius to thickness ratio equal to R_b/h and made of the same material.

The initial post-buckling behaviour is given by an asymptotically exact expression for the load

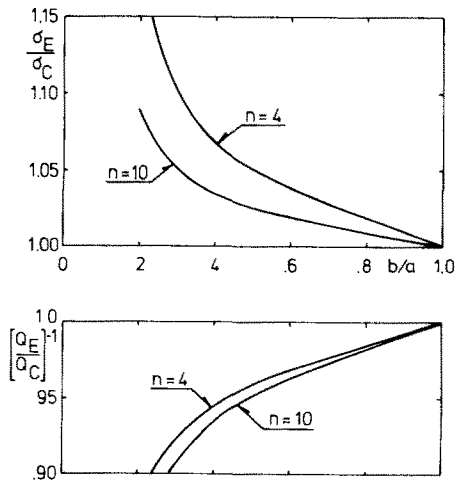

Fig. 2. Critical stress and corresponding axial wave length in elliptical cylinders with aspect ratio b/a. ($R_b/h = 200$, $\sigma_C/\sigma_y = 1.034$, $\sigma_y/E = 0.0025$, $\nu = 0.3$).

parameter λ in terms of the buckling mode amplitude ξ of the form[9]

$$\lambda = \lambda_c + \lambda_1 \xi + \lambda_2 \xi^{1+\beta} + \cdots \tag{3.4}$$

for $\xi \geq 0$. Here, we normalize the buckling mode so that for $\xi = 1$ the maximum deflection w is equal to the shell thickness. The initial slope λ_1 is determined from the requirement that initially at bifurcation plastic loading occurs everywhere in the current plastic zone, except in at least one point where neutral loading takes place. As ξ grows, a region of elastic unloading spreads into the material from each point of neutral loading, and the effect of these elastic unloading regions is accounted for in the third term of the expansion (3.4). Figure 3 indicates the shape of these elastic unloading regions that start on the inside of the shell at the points of maximum inward deflection.

When unloading starts at isolated points, as shown in Fig. 3, we find $\beta = 1/3$, whereas for the limit of the circular cylindrical shell, where unloading starts along circles on the inside surface, we find $\beta = 2/5$. Since in all cases we find $\lambda_2 < 0$, the truncated expansion (3.4) can be used to estimate the maximum support load λ_{max} and the corresponding buckling mode amplitude ξ_{max}. It should be emphasized that the values of λ_{max} and ξ_{max} obtained in this manner are not asymptotic in any sense, since the maximum always occurs at a finite, perhaps small, valur of ξ. The bifurcation analysis and the initial post-bifurcation expansion have been computed with 5, 10 and 20 elements, respectively, to represent one quarter of the shell circumference, but only minor differences result from this variation of the mesh. The values of the constants σ_E, λ_1, λ_2, λ_{max} and ξ_{max} given in Table 1 for a number of cases, have been computed with 10 elements.

Fig. 3. Shape of elastic unloading regions (shell thickness exaggerated).

b/a	R_b/h	σ_y/E	n	σ_E/σ_y	λ_1/λ_c	λ_2/λ_c	β	λ_{max}/λ_c	ξ_{max}
.5	200	.0025	10	1.058	2.75	-11.7	1/3	1.0037	.0054
.5	200	.0025	4	1.131	2.83	-10.9	1/3	1.0052	.0074
.8	200	.0025	10	1.044	3.02	-14.9	1/3	1.0027	.0035
.8	200	.0025	4	1.098	3.07	-13.4	1/3	1.0039	.0051
1.0	200	.0025	10	1.034	3.23	-22.7	2/5	1.0030	.0033
1.0	200	.0025	4	1.078	3.27	-19.4	2/5	1.0047	.0050

Table 1. Constants in asymptotic post-bifurcation expansion for various elliptical cylinders made of material with $\sigma_y/E = 0.0025$, $\nu = 0.3$

In the cases considered here bifurcation does not occur far into the plastic range, and thus the bifurcation predictions of J_2-flow theory are only a little above those of J_2-deformation theory. For the cylinders of Table 1 this discrepancy is below one half per cent.

4. NUMERICAL COMPUTATION OF IMPERFECTION-SENSITIVITY

The behaviour of a shell with initial imperfections is computed numerically by an incremental procedure. At each stage of the loading history incremental equilibrium is expressed in terms of the following variational principle: Among all displacement increment fields that satisfy the kinematical boundary conditions, the actual displacement increments satisfy

$$\delta I = 0 \tag{4.1a}$$

$$\begin{aligned} I = \frac{1}{2}\int_0^{s_M}\int_0^{x_M} [&H_{(1)}^{\alpha\beta\gamma\delta}\dot{\epsilon}_{\alpha\beta}\dot{\epsilon}_{\gamma\delta} + 2H_{(2)}^{\alpha\beta\gamma\delta}\dot{\epsilon}_{\alpha\beta}\dot{\kappa}_{\gamma\delta} + H_{(3)}^{\alpha\beta\gamma\delta}\dot{\kappa}_{\alpha\beta}\dot{\kappa}_{\gamma\delta} \\ &+ N^{\alpha\beta}\{a^{\gamma\delta}(\dot{v}_{\gamma,\alpha} - d_{\gamma\alpha}\dot{w})(\dot{v}_{\delta,\beta} - d_{\delta\beta}\dot{w}) \\ &+ (\dot{w}_{,\alpha} + d_\alpha{}^\gamma \dot{v}_\gamma)(\dot{w}_{,\beta} + d_\beta{}^\delta \dot{v}_\delta)\}] \, dx \, ds - \dot{\lambda}\left[\int_0^{s_M} N_0{}^{11}\dot{v}_1 \, ds\right]_{x=0}^{x_M}. \end{aligned} \tag{4.1b}$$

Integrations in the circumferential direction are taken over one quarter of the circumference, since consideration is restricted to deformations that are symmetric with respect to both the minor and the major axes. In the axial direction the deformation pattern is taken to be periodic, and integration is performed over one half period, assuming symmetry conditions at $x = 0, x_M$. The moduli $H_{(i)}^{\alpha\beta\gamma\delta}$ are defined by (2.11), $N^{\alpha\beta}$ is the current membrane stress tensor, $\dot{\lambda}$ is the prescribed increment of the load parameter, and expressions for the incremental strain quantities in terms of current displacements and displacement increments are obtained from (2.4) and (2.5).

The numerical method employed to solve eqn (4.1) is based on expanding the displacements in terms of trigonometric functions in the axial direction, and using a one-dimensional finite element approximation in the circumferential direction. Thus, the displacements are taken of the form

$$\begin{Bmatrix} v_1 \\ v_2 \\ w \end{Bmatrix} = \begin{Bmatrix} U^{(1)}(s) & x/x_M \\ V^{(1)}(s) & \\ W^{(1)}(s) & \end{Bmatrix} + \sum_{n=2}^{N} \begin{Bmatrix} U^{(n)}(s) & \sin(q_n x) \\ V^{(n)}(s) & \cos(q_n x) \\ W^{(n)}(s) & \cos(q_n x) \end{Bmatrix} \tag{4.2}$$

where the functions $U^{(i)}(s)$, $V^{(i)}(s)$ and $W^{(i)}(s)$ are approximated by Hermitian cubics within each finite element.

To avoid numerical difficulties around the maximum load a special technique is employed, which is based on using a few of the nodal displacement increments as initially prescribed increments. For this purpose we chose the constant axial edge displacement $\dot{U} = \dot{U}^{(1)}(s)$ and one normal node deflection $\dot{W}$ (for example the deflection in the mode $W^{(i)}(s)$ corresponding to the bifurcation mode wavelength, taken at the point of maximum deflection). Now, the variational eqn (4.1) is solved with two different sets of prescribed displacement increments, $\dot{U} = 1$, $\dot{W} = 0$ and $\dot{U} = 0$, $\dot{W} = 1$, and finally these two finite element solutions are used as trial functions in a Rayleigh Ritz solution to obtain the values of $\dot{U}$ and $\dot{W}$ corresponding to a given load increment $\dot{\lambda}$. In these two Rayleigh Ritz equations instead of always prescribing $\dot{\lambda}$ we prescribe that of the three parameters $\dot{U}$, $\dot{W}$, $\dot{\lambda}$ that is numerically largest in the previous increment and solve for the two remaining parameters. This procedure also makes it easy to pass maxima, at which both $\dot{\lambda}$ and $\dot{U}$ change sign nearly simultaneously, as is often the case for nearly perfect axially compressed cylinders in the vicinity of the bifurcation point. It should be emphasized that introducing the additional solution of (4.1) and the Rayleigh–Ritz solution adds very little to the computer time required for each increment.

The integrals in eqns (4.1) and (2.11) are evaluated numerically as follows. In the circumferential direction 4 point Gaussian quadrature is used within each element, while in the axial direction the interval $x = 0, x_M$ is divided in as many subintervals as the largest number of half-waves in (4.2) and 4 point Gaussian quadrature is used within each subinterval. Through the thickness Simpson's rule is used, with 7 points.

The active branch of the tensor of moduli (2.8) to be used in (2.11) is determined in each increment as follows. If the stress state at an integration point is on its current yield surface, the plastic branch is taken to be active. If $\dot{\sigma}_e$ for that integration point turns out to be negative, the elastic branch is taken to be active in the next loading increment. This procedure is sufficiently accurate if small increments are used and if the transition from loading to unloading, or vice versa, occurs only once or twice during the loading history.

Results of numerical computations are shown in Figs. 4–7. The initial stress free imperfections considered are in the shape of the cirtical bifurcation mode with $\bar{\xi}_1$ denoting the ratio between the amplitude and the shell thickness. The figures give the load parameter λ as a function of the end-shortening Δ, with these variables normalized against their values λ_c and Δ_c at the bifurcation point according to DMV shell theory.

The first computations for shells with aspect ratio $b/a = 0.5$ (Figs. 4–6) are made with $N = 3$ in eqn (4.2) by choosing the wave numbers $q_2 = Q_E$, $q_3 = 2Q_E$, of which the first is that of the bifurcation mode and of the specified initial imperfection. It has been checked for a few of the computations that the result is not changed by introducing an extra mode with $q_4 = Q_E/2$ and with a small initial deflection $\bar{\xi}_2 = 0.1\bar{\xi}_1$. In the circumferential direction 5 elements are used, which is judged sufficient since only rather little is gained compared with a 2 element computation.

The post-bifurcation behaviour of the perfect shell is computed numerically as the behaviour of a shell with very small initial imperfections. For the oval shells considered in Figs. 5 and 6 that

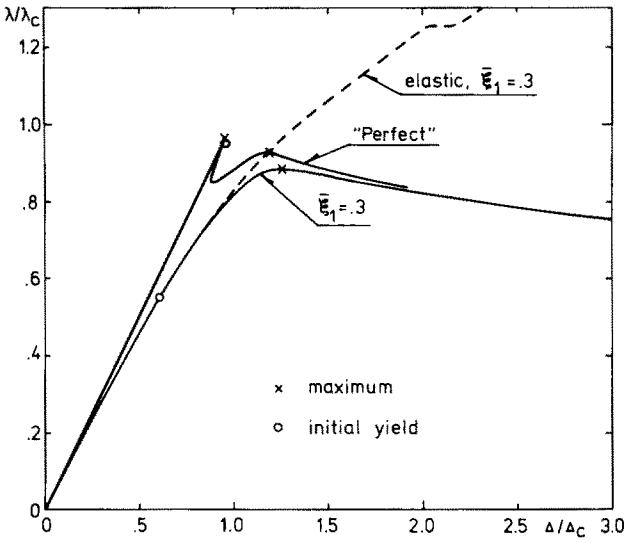

Fig. 4. Load vs end-shortening for elliptic cylindrical shell that bifurcates in the elastic range ($b/a = 0.5$, $R_b/h = 286$, $\sigma_E/\sigma_y = 0.92$, $\sigma_y/E = 0.0025$, $n = 10$, $\nu = 0.3$).

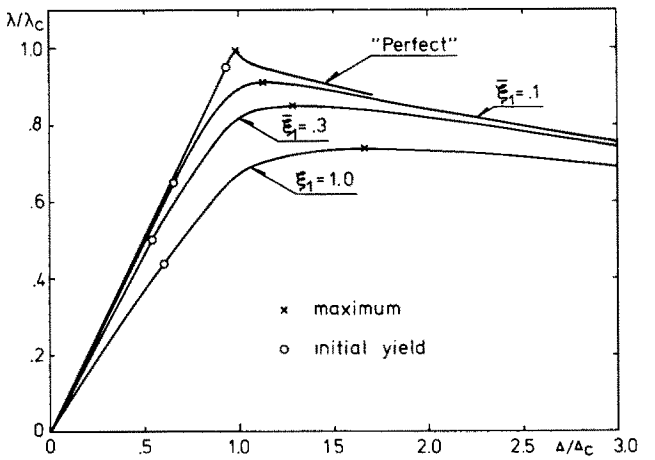

Fig. 5. Load vs end-shortening for elliptic cylindrical shell that bifurcates in the plastic range ($b/a = 0.5$, $R_b/h = 200$, $\sigma_E/\sigma_y = 1.058$, $\sigma_y/E = 0.0025$, $n = 10$, $\nu = 0.3$).

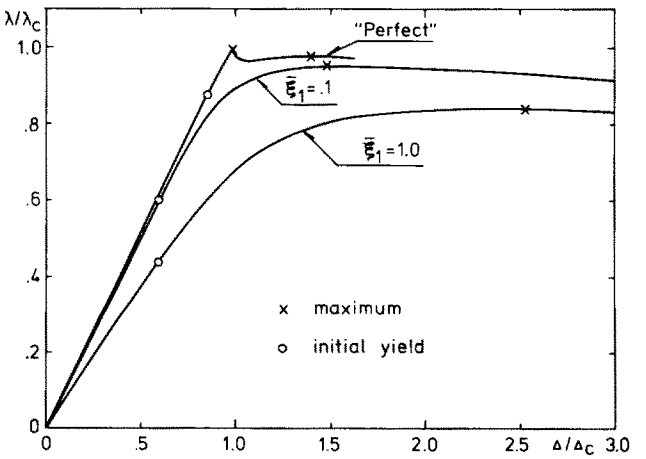

Fig. 6. Load vs end-shortening for elliptic cylindrical shell that bifurcates in the plastic range ($b/a = 0.5$, $R_b/h = 200$, $\sigma_E/\sigma_y = 1.131$, $\sigma_y/E = 0.0025$, $n = 4$, $\nu = 0.3$).

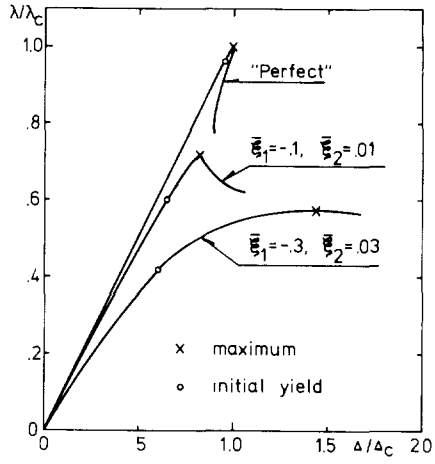

Fig. 7. Load vs end-shortening for circular cylindrical shell that bifurcates in the plastic range ($R/h = 200$, $\sigma_c/\sigma_y = 1.034$, $\sigma_y/E = 0.0025$, $n = 10$, $\nu = 0.3$).

bifurcate in the plastic range the numerical results confirm the general trends of the asymptotic analysis, although the numerically obtained values of λ_{max}/λ_c and ξ_{max} are somewhat larger than those given in Table 1. Also the initial spreading of elastic unloading regions starting from the points of maximum inward deflection, as shown in Fig. 3, is confirmed numerically. Furthermore, the numerical computations show that after a small finite mode deflection a second set of unloading regions start to spread into the material from the points of maximum outward buckling deflection.

The shell in Fig. 4 bifurcates in the elastic range with a slightly lower buckling load predicted by the more accurate shell theory than that of DMV-theory. Plastic yielding starts very shortly after bifurcation, but even so the steep initial descent of the post-buckling path succeeded by an interval of increasing load is found in agreement with the behaviour of the elastic shell. However, due to the effect of plasticity this secondary increase levels off before again reaching the bifurcation load, and a second maximum is passed. For an imperfection $\bar{\xi}_1 = .3$ the initial part of the elastic solution is shown to illustrate the well-known carrying capacity above the level of bifurcation, where the load is mainly carried by the strongly curved regions in which buckles grow less rapidly. When the shell material is elastic-plastic, yielding starts quite early at the peaks of the buckles in the region of minimum curvature, and a maximum is reached shortly after the strongly curved regions at the ends of the major axis have started to yield.

The shell considered in Fig. 5 is somewhat thicker than the first shell, so that bifurcation occurs in the plastic range. Now, the sharp initial drop in post-bifurcation load has vanished, and the load decreases monotonically with increasing end-shortening after bifurcation. The computations for shells with various imperfection amplitudes show that the carrying capacity above the bifurcation load known from elastic shells is now replaced by a moderate imperfection-sensitivity. This imperfection-sensitivity is still far less severe than that of an elastic-plastic spherical shell under external pressure[15], but is comparable with the imperfection-sensitivity of an axially compressed rectangular plate made of the same elastic-plastic material[16].

For a more strain-hardening material, with $n = 4$ instead of $n = 10$, the same shell is less imperfection-sensitive (Fig. 6), but still the load carrying capacity does not exceed the bifurcation load. In this case the post-bifurcation load of the perfect shell varies initially like that of Fig. 5, but then starts to increase slightly again before reaching a second maximum.

As the aspect ratio b/a increases towards unity from the relatively small value, $b/a = 0.5$, considered in the previous figures, the post-buckling load carrying capacity above the bifurcation load vanishes for elastic shells, and accordingly the imperfection-sensitivity increases for elastic-plastic shells. Then the earlier mentioned extra mode with double wavelength in the axial direction becomes increasingly important, since the maximum load computed by the usual three modes in (4.2) will be reduced due to a bifurcation into the double wavelength mode with a short-wave pattern in the circumferential direction. This behaviour has been found for a shell

with aspect ratio $b/a = 0.9$ by a computation with relatively few elements. However, in order to avoid the rather costly computations with $N = 4$ in eqn (4.2) and with sufficiently many finite elements in the circumferential direction, it is preferred here to show a few results for the special case of a circular cylinder.

The circular cylindrical shell considered in Fig. 7 has an axisymmetric imperfection of amplitude $\bar{\xi}_1$ and an asymmetric circumferentially periodic imperfection of amplitude $\bar{\xi}_2$, such that a sufficiently accurate computation can be made with only two elements over one half wave length in the circumferential direction. These two types of imperfections are specified for $q_2 = Q_C$ and $q_4 = Q_C/2$, respectively, in eqn (4.2), and the asymmetric imperfection is chosen with approximately the same circumferential as axial wave length. The perfect shell behaves initially as predicted by the asymptotic analysis (Table 1), with bifurcation into the axisymmetric mode and a small buckling mode deflection before the maximum load is reached. However, slightly after the maximum load a secondary bifurcation occurs into the asymmetric mode, which results in a rapid decrease of post-buckling load rather similar to the behaviour known from the elastic range. The curve computed for $\bar{\xi}_1 = -0.1$ and $\bar{\xi}_2 = 0.01$ shows a very strong sensitivity to small initial imperfections, which is entirely due to interaction of the axisymmetric and asymmetric modes used as imperfections. However, for the larger imperfections, $\bar{\xi}_1 = -0.3$ and $\bar{\xi}_2 = 0.03$, the growth of the chosen asymmetric mode ceases shortly after initial yielding, and the axisymmetric deformation is completely dominant around the maximum load.

5. CONCLUSION

An analysis of long oval cylindrical shells under axial compression has shown that the post-buckling behaviour known from the elastic range is significantly changed by the effect of plastic yielding. For elastic shells with sufficiently eccentric cross-sections the unstable initial post-buckling behaviour is succeeded by an interval of increasing load as the buckles spread from the ends of the minor axis into the regions of higher curvature, and the final collapse load is above the initial bifurcation load. In the plastic range the strongly curved regions are weakened by the material non-linearity even before the buckles spread into these regions, and therefore the reserve of post-buckling stiffness is not available in cases where plastic yielding takes place. Thus, the high post-buckling support load of the eccentric, elastic shell is replaced by a moderate imperfection-sensitivity of the plastic shell. For decreasing eccentricity of the cross-section the imperfection-sensitivity increases to be rather strong in the special case of a circular cylindrical shell.

REFERENCES

1. J. W. Hutchinson, Buckling and initial postbuckling behaviour of oval cylindrical shells under axial compression. *J. Appl. Mech.* **35**, 66–72 (1968).
2. J. Kempner and Y. -N. Chen, Large deflections of an axially compressed oval cylindrical shell. *Proc. 11th Int. Congr. Appl. Mech.* (Edited by H. Görtler), pp. 299–306. Springer-Verlag, Berlin (1966).
3. J. Kempner and Y. -N. Chen, Postbuckling of an axially compressed oval cylindrical shell. *Proc. 12th Int. Congr. Appl. Mech.* pp. 246–256. Springer-Verlag, Berlin (1969).
4. B. O. Almroth, F. A. Brogan and M. B. Marlowe, Collapse analysis for elliptic cones. *AIAA J.* **9**, 32–37 (1971).
5. R. C. Tennyson, M. Booton and R. D. Caswell, Buckling of imperfect elliptical cylindrical shells under axial compression. *AIAA J.* **9**, 250–255 (1971).
6. G. Feinstein, B. Erickson and J. Kempner, Stability of oval cylindrical shells. *Experimental Mechanics* **11**, 514–520 (1971).
7. J. Kempner and Y. -N. Chen, Buckling and initial post-buckling of oval cylindrical shells under combined axial compression and bending. *Transactions New York Academy of Sciences* **36**, Series II, No. 2, 171–191 (1974).
8. J. W. Hutchinson, Post-bifurcation behavior in the plastic range. *J. Mech. Phys. Solids* **21**, 163–190 (1973).
9. J. W. Hutchinson, Plastic buckling. *Advances in Applied Mechanics* (Edited by C. S. Yih), Vol. 14, pp. 67–144. Academic Press, New York (1974).
10. F. Niordson, *Indledning til skalteorien*. Technical University of Denmark, Lyngby (1974).
11. W. T. Koiter, On the nonlinear theory of thin elastic shells. *Proc. Kon. Ned. Ak. Wet.* **B69**, 1–54 (1966).
12. R. Hill, A general theory of uniqueness and stability in elastic-plastic solids. *J. Mech. Phys. Solids* **6**, 236–249 (1958).
13. R. Hill, Bifurcation and uniqueness in non-linear mechanics of continua. *Problems of Continuum Mechanics* (S.I.A.M. Philadelphia), 155–164 (1961).
14. W. T. Koiter, Over de stabiliteit van het elastisch evenwicht. Thesis, Delft, H. J. Paris, Amsterdam (1945). English transl.: NASA TT F-10, 833, (1967); and AFFDL-TR-70-25 (1970).
15. J. W. Hutchinson, On the postbuckling behavior of imperfection-sensitive structures in the plastic range. *J. Appl. Mech.* **39**, 155–162 (1972).
16. A. Needleman and V. Tvergaard, An analysis of the imperfection-sensitivity of square elastic-plastic plates under axial compression. *Int. J. Solids Structures* **12**, 185–201 (1976).